Korean J. Chem. Eng., 33(7), 2034-2041 (2016)
DOI: 10.1007/s11814-016-0065-y

pISSN: 0256-1115
eISSN: 1975-7220

The catalytic performance of methylation of naphthalene with methanol over SAPO-11 zeolites synthesized with different Si content

Xiaoxiao Wang*, Fang Guo**, Xianxian Wei***, Zhenmin Liu*, Wei Zhang**, Shaoqing Guo***,†, and Liangfu Zhao**,†**

*Taiyuan University of Science and Technology, School of Chemical and Biological Engineering, Taiyuan 030024, P. R. China
**Institute of Coal Chemistry, Chinese Academy of Sciences, Taiyuan 030001, P. R. China
***Taiyuan University of Science and Technology, College of Environment and Safety, Taiyuan 030024, P. R. China
****Jin Zhong University, College of Chemistry and Chemical Engineering, Yuci 030619, P. R. China
(*Received 30 June 2015 • accepted 4 March 2016*)

Abstract−A series of SAPO-11 zeolites with different Si contents were prepared by hydrothermally synthesized method. They were characterized by ICP, XRD, SEM, FT-IR, N_2 adsorption-desorption, NH_3-TPD and ^{29}Si MAS NMR, and evaluated by the methylation of naphthalene with methanol to 2,6-dimethylnaphthalene (2,6-DMN). According to XRD and SEM results, the crystallinity of SAPO-11 sample increased with increase of the Si content until the SiO_2/Al_2O_3 ratio was up to 0.2. However, a reduction in the crystallinity was observed with further increase of the Si content of the synthesis. N_2 adsorption-desorption results showed that all the samples possessed micropores and secondary mesopores. SAPO-11 sample with SiO_2/Al_2O_3 ratio of 0.2 exhibited the largest secondary mesopores size distributions. NH_3-TPD and ^{29}Si MAS NMR showed that the Si content was incorporated into the framework affecting not only the acid sites but also the acid strength of SAPO-11. SAPO-11 with SiO_2/Al_2O_3 ratio of 0.2 presented the high catalytic performances for the methylation of naphthalene, which was mainly attributed to the amount of secondary mesopores in the SAPO-11 zeolite.

Keywords: SAPO-11, Si Content, Pore Structure, Methylation of Naphthalene

INTRODUCTION

2,6-Dimethylnaphthalene (2,6-DMN) is an important intermediate in the synthesis of polyethylene naphthalate (PEN). As a novel polyester, it exhibits superior properties including high tensile strength, heat resistance and gas barrier property as compared with polyethylene terephthalate [1,2]. The synthesis of 2,6-DMN by the methylation of naphthalene with methanol over zeolites has attracted more attention due to its simple synthetic route and low production cost. Several aluminosilicate zeolites such as ZSM-5, HY, ZSM-12 and Beta have been studied in the synthesis of 2,6-DMN by the methylation of naphthalene with methanol [3-6]. However, few reports concerned silicoaluminophosphate zeolites. Among silicoaluminophosphate zeolites, SAPO-11 has proven to be effective with high catalytic activity and selectivity of 2,6-DMN in the methylation of naphthalene [7,8].

Microporous aluminophosphate zeolites $AlPO_4$-n were first developed by Union Carbide Corporation in 1982. Soon afterwards, SAPO-n was prepared by incorporation of Si atoms into the $AlPO_4$-n framework. The structure of SAPO-11 is similar to that of $AlPO_4$-11, which consists of a one-dimensional ten membered-ring channel system with a pore size of 0.39 nm×0.64 nm [9,10]. SAPO-11 exhibits milder acidity due to the presence of phosphorus and its acidic properties depend on the content, location and distribution of Si atoms. It is proposed that Si atoms incorporate into the $AlPO_4$-11 structure by three different substitution mechanisms [11,12]: the first mechanism (SM1) is the substitution of a Si atom for an Al atom, which could not occur practically due to the formation of undesirable Si-O-P linkages. The second mechanism (SM2) is the substitution of a P atom by a Si atom, which produces an isolated Si (4Al) site and gives rise to acid sites with weak strength. SM3 mechanism involves the substitution of a pair of Al and P by two Si atoms, which cannot occur independently because of the formation of undesirable Si-O-P linkages like SM1. SM3 can take place by the combination with SM2 to avoid the formation of Si-O-P. Such substitution forms an Si island, which consists of Si (4Si) site and Si (n Al, 4-n Si, 0<n<4) environments. Although the inside Si atoms (Si (4Si)) in Si islands hardly generate acidity, acid sites with medium strength could be produced from the border of Si domains (Si (n Al, 4-n Si, 0<n<4)).

Since the origin of the protonic acidity in SAPO-11 is related to the presence of Si atoms, Si content plays an important role in the synthesis of SAPO-11, and the different Si content maybe leads to different physicochemical properties and different catalytic performance for SAPO-11. However, studies about the influence of Si content on the catalytic performances of SAPO-11 have not been reported in the methylation of naphthalene so far. In this paper, a series of SAPO-11 zeolites were synthesized with different Si content by hydrothermal method to investigate the influence of Si content on the physicochemical and catalytic performance of SAPO-

†To whom correspondence should be addressed.
E-mail: guosq@sxicc.ac.cn, lfzhao@sxicc.ac.cn

11 in the methylation of naphthalene. The physicochemical properties of the SAPO-11 samples were characterized by ICP, XRD, SEM, FT-IR, N_2 adsorption-desorption, NH_3-TPD and ^{29}Si MAS NMR, and the catalytic performance of these samples was also studied for the methylation of naphthalene with methanol.

EXPERIMENTAL

1. Catalyst Preparation

In the synthesis of SAPO-11, 72% pseudoboehmite (Zibo Yinghe Chemical Co., Ltd.), 85% orthophosphoric acid (Shandong Zhenhua Ind. Co., Ltd.), 30% silica sol with the size distribution: 10-20 nm (Guangzhou Fuer Chemical Technoligy Co., Ltd.) and Di-n-propylamine (DPA) (Sinopharm Chemical Reagent Co., Ltd.) act as an aluminium source, a phosphorus source, a silicon source and an organic template, respectively. SAPO-11 was synthesized hydrothermally with a composition of $1.0Al_2O_3 : 1.0P_2O_5 : XSiO_2 : 1.2DPA : 49H_2O$, X=0, 0.1, 0.2, 0.3 and 0.4. The detailed procedures were as follows.

Orthophosphoric acid was added to deionized water, and then pseudoboehmite and silica sol were added dropwise. The mixture was stirred for 3 h to become homogeneous and then the DPA was added. The synthesis mixture was stirred for 2 h to form the synthesis gel. The gel was sealed in the Teflon-lined stainless steel autoclave and heated at 200 °C for 24h. After crystallization, the as-synthesized sample was obtained after filtration, washing, and drying at 120 °C for 12 h. Calcination was at 550 °C for 6 h to remove organic template. The samples prepared with SiO_2/Al_2O_3 molar ratio of 0, 0.1, 0.2, 0.3 and 0.4 were denoted as SP-0, SP-0.1, SP-0.2, SP-0.3, SP-0.4, respectively.

2. Catalyst Characterization

The elemental compositions of the samples were determined by inductively coupled plasma-optical (ICP) emission spectroscopy (Perkin-Elmer ICP OPTIMA-3000).

X-ray powder diffraction (XRD) analysis was performed on RigakuD/maxrB X-ray diffractometer. Diffraction patterns were recorded with Cu Ka radiation at 40 kV and 100 mA in the scan range between 5° and 50° to identify the phase structure of the sample. Scanning electron microscopy (SEM) was performed with a LEO-435VP scanning electron microscopy operated at 20 kV and 50 PA. Fourier transform infrared spectroscopy (FT-IR) spectra of the samples were recorded with a Nicolet 380 FT-IR spectrometer.

The textural properties of the samples were derived from N_2 adsorption-desorption measurement on Micromeritics Tristar 3000. In each case, the sample was outgassed under vacuum at 300 °C for 3 h before N_2 adsorption. The specific surface area was calculated according to BET method and the volume of porous was obtained by t-plot analysis of the adsorption isotherm. The pore size distributions were analyzed by corresponding Horvath-Kawazoe (HK) and Barrett-Joyner-Halenda (BJH) methods.

The acidity was examined by temperature programmed desorption of ammonia (NH_3-TPD) techniques, which was carried out in a flow system with a thermal conductivity detector. All samples were preheated from room temperature to 500 °C in argon flow and kept at 500 °C for 1 h, which was followed by NH_3 saturation in a flowing NH_3/Ar stream at 40 °C for 5 min. Evacuation at 40 °C for 40 min was carried out to remove physically adsorbed NH_3 and then the catalyst was heated to 600 °C at a linear heating rate of 10 °C/min, and the detector signal of NH_3 was recorded.

^{29}Si MAS NMR experiments involved using a Varian infinity-plus 300 NMR. All ^{29}Si MAS NMR spectra were recorded at 79.5 MHz using 2.0 μs pulse with 3.0 s recycle delay and 7120 scans.

3. Catalyst Evaluation

The experiments were performed in a continuous flow fixed-bed reactor equipped with 20 mm diameter and 600 mm length stainless steel tube. 2.5 g of 20-40 mesh zeolite catalysts were loaded in the reaction tube. The reaction mixture was fed into the reactor by a quantity measuring pump and the pressure was kept by N_2. The weight hourly space velocity (WHSV) of naphthalene was 0.19 h^{-1} in all experiments. The reaction temperature was 400 °C and the liquid reactant including naphthalene, methanol and mesitylene (solvent) in a molar ratio of 1 : 5 : 3.5 was preheated before passing to the reactor. The reaction products were analyzed by gas chromatography (GC9560) with a Beta-Dex120 capillary column. The conversion of naphthalene was calculated as follows:

$$\text{Naphthalene conv. (\%)} = \left(\frac{n_{N,0} - n_N}{n_{N,0}}\right) \times 100$$

where $n_{N,0}$ and n_N are the molar percentage of naphthalene before and after the reaction. The product distribution include the corresponding molar percentages of ethylnaphthalene (EN), methylnaphthalene (MN), dimethylnaphthalene (DMN) and trimethylnaphthalenes (TMN) in the total product mixture.

The selectivity of 2,6-DMN is the corresponding molar percentage in the sum of all DMN isomers. And the selectivity of DMN is the ratio between the sum of molar percentage of all the DMN isomers and the sum of the molar percentages of the total products. The definition of 2,6-DMN distribution is as follows: 2,6-DMN distribution=the selectivity of 2,6-DMN×the selectivity of DMN. 2,6-/2,7-DMN stands for the molar ratio of 2,6-DMN to 2,7-DMN. 2,6-DMN yield=(naphthalene conversion×2,6-DMN distribution)/100%.

Table 1. Molar composition of the initial gel and as-synthesized SAPO-11 samples

Sample	Starting gel composition Molar composition	Product composition	Al/P
SP-0.1	$1.0P_2O_5 : 1.0Al_2O_3 : 0.1SiO_2$	$(Si_{0.061}Al_{0.502}P_{0.437})O_2$	1.15
SP-0.2	$1.0P_2O_5 : 1.0Al_2O_3 : 0.2SiO_2$	$(Si_{0.118}Al_{0.467}P_{0.415})O_2$	1.13
SP-0.3	$1.0P_2O_5 : 1.0Al_2O_3 : 0.3SiO_2$	$(Si_{0.134}Al_{0.456}P_{0.410})O_2$	1.11
SP-0.4	$1.0P_2O_5 : 1.0Al_2O_3 : 0.4SiO_2$	$(Si_{0.167}Al_{0.472}P_{0.361})O_2$	1.30

RESULTS AND DISCUSSION

1. Physicochemical Property

1-1. ICP

Table 1 shows the elemental composition (Al, Si and P) of the initial synthesis gel and the corresponding final SAPO-11 samples' obtained by the results of ICP analysis. A deviation of elemental composition (Al, Si and P) of the products was observed from that of the gel mixture. The Si content of the samples was lower than that of the gels, which indicates that some Si atoms were lost during the synthesis. The Al/P ratio of the products increases to higher values than the initial synthesis gel ($Al/P_{gel}=1$), indicating the replacement of P atoms for Si atoms in the prepared SAPO-11 samples' structure.

1-2. XRD

Fig. 1 presents XRD patterns of as-synthesized samples of SP-0, SP-0.1, SP-0.2, SP-0.3 and SP-0.4. As shown, the characteristic peaks of the SAPO-11 phase (2θ=8.15°, 9.40°, 13.20°, 15.57°) are observed for all the as-synthesized samples, which are identical to the pure SAPO-11 material [13]. These results suggest that all of the samples are phase-pure materials with AEL topology and do not contain any additional microporous or dense crystalline phases. Also,

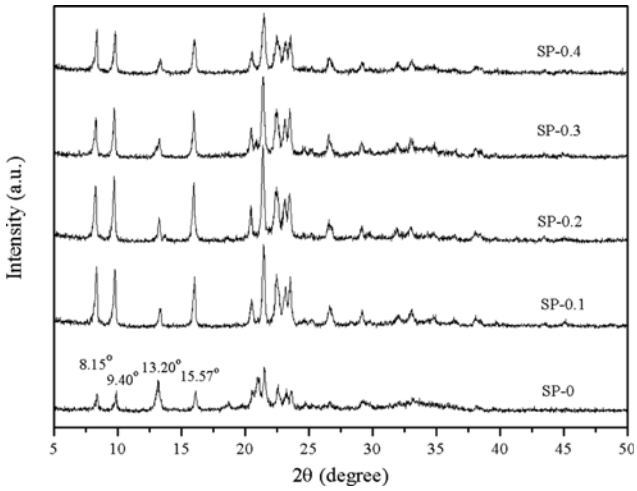

Fig. 1. XRD patterns of SAPO-11 samples synthesized with different Si contents.

$AlPO_4$-11 phase was formed when the SiO_2/Al_2O_3 molar ratio of the starting gel was equal to 0, which indicates that SAPO-11 and $AlPO_4$-11 have the same characteristic peaks. Fig. 1 shows that the

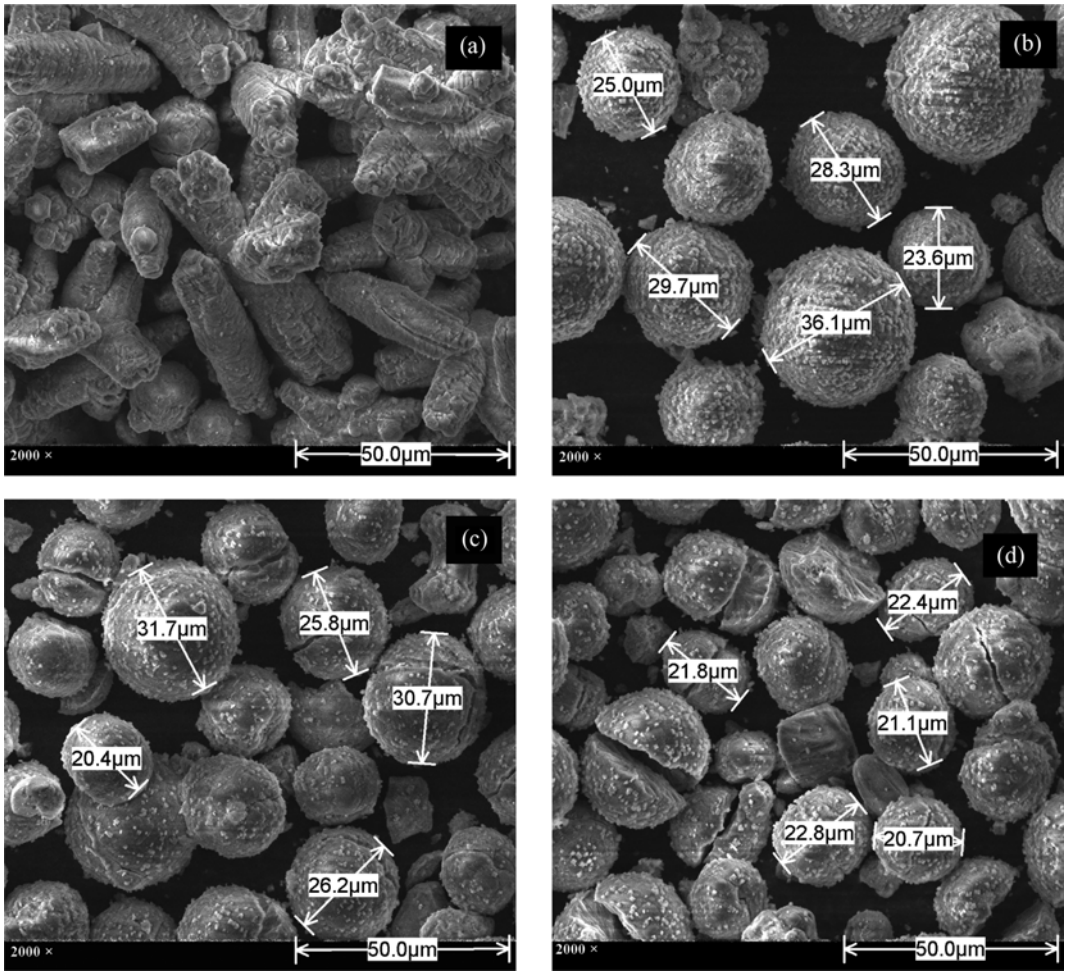

Fig. 2. SEM images of as-synthesized SAPO-11 samples (a) SP-0.1, (b) SP-0.2, (c) SP-0.3, (d) SP-0.4.

intensity and crystallinity of the samples are different. The crystallinity of SAPO-11 samples is the highest when the SiO_2/Al_2O_3 molar ratio of the starting gel is 0.20, and then the crystallinity of samples reduces with the increase of Si content. This implies that SAPO-11 is probably contaminated by amorphous phase when Si content is high.

1-3. SEM

SEM results of the as-synthesized samples are presented in Fig. 2(a)-(d). The morphology of SP-0.1 is cylindrical and long, and may represent aluminophosphate material [14], which was caused by that the amount of Si atoms of SP-0.1 was less than that of the synthesized samples. With more Si atoms incorporated into the $AlPO_4$ framework, uniform spherical-like crystals were obtained for SP-0.2, SP-0.3 and SP-0.4. And SP-0.2 had the largest particle size with the best crystallinity, which agrees with the results of XRD. SP-0.4 had the smallest particle size. This is because excessive Si atoms are expelled from the framework during the formation process of SAPO-11, and amorphous materials may be formed with the increase of Si content, which affects the morphology of the as-synthesized samples.

1-4. FT-IR Spectra

Fig. 3 shows FT-IR spectra of as-synthesized samples. According to the literature [15], all peaks are assigned as follows: the bands appearing between 3,500-4,000 cm^{-1} are assigned to the hydroxyl vibration. 1,121 cm^{-1} arising from the asymmetric stretching vibration of inner tetrahedra; 706 cm^{-1} ascribed to the symmetric stretching vibration of inner tetrahedra; 630 cm^{-1} and 556 cm^{-1} is due to the deformation vibration of four-membered ring and the deformation vibration of six-membered ring, respectively. The 417 cm^{-1} corresponds to the deformation vibration of inner tetrahedra. As shown in Fig. 3(a) all the framework vibration peaks weaken and gradually expand with the improving of Si content, which may be because the bond length of the Si-O linkage (0.160 nm) is longer than that of the P-OH linkage (0.153 nm), and thus the framework vibration peaks appear a broadening phenomenon. Fig. 3(b) shows that the band appearing at 3,732 cm^{-1} is assigned to Si-OH bonds and the one at 3,673 cm^{-1} is assigned to to P-OH bonds. There are two bands at 3,628 cm^{-1} and 3,800 cm^{-1}, which correspond to the Si-OH-Al bands and Al-OH bands, respectively [16]. SP-0.4 exhibits a slightly larger number of defects sites of Si-OH bonds probably due to higher Si atoms incorporation.

1-5. N_2 Adsorption-desorption Characterization

Table 2 presents the pore structure parameters of SAPO-11 samples prepared with different Si content. As seen, there is not a direct relationship between the BET surface area and the Si content of as-synthesized samples. Regarding XRD pattern of the sample SP-0.2, it has the highest crystallinity among samples but not the highest surface area, which belongs to SP-0.3. The reason is that the new pore could be probably generated due to the lower crystallinity, leading to higher surface area. It's worth noting that the micropore volume of as synthesized samples tends to drop with

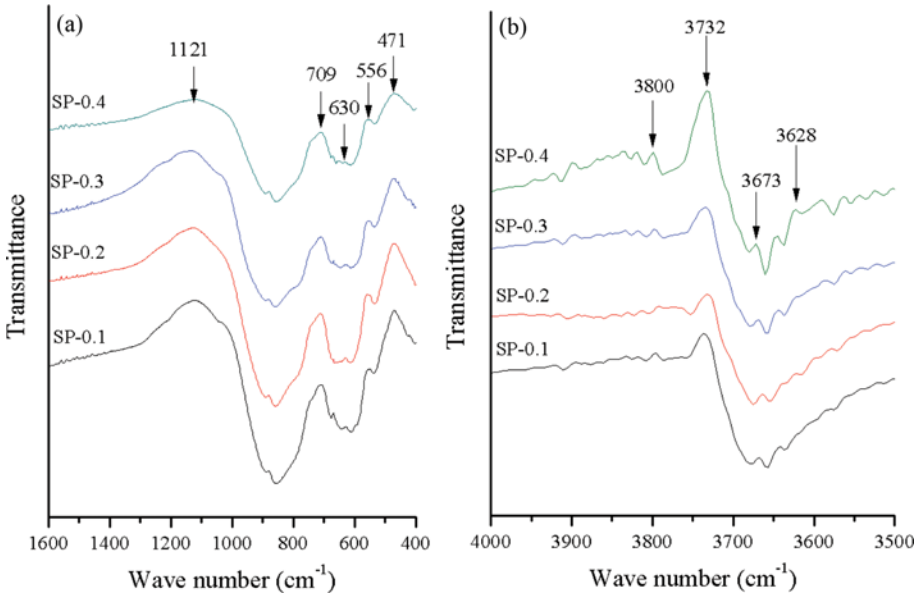

Fig. 3. FT-IR spectra of as-synthesized SAPO-11 samples.

Table 2. The pore structure parameters of SAPO-11 samples

Sample	Surface area, m^2/g			Pore volume, cm^3/g		
	BET	Micropore	External	Total	Micropore	Mesopore
SP-0.1	149.6	96.6	53	0.116	0.053	0.063
SP-0.2	145.1	80.1	65	0.125	0.043	0.082
SP-0.3	152.2	91.2	61	0.108	0.042	0.066
SP-0.4	141.8	82.8	59	0.097	0.038	0.059

increasing Si content. It indicates that the improving of Si content leads to more and more Si atoms, which are not incorporated into the $AlPO_4$-11 framework. And thus these Si atoms formed non-framework materials in the micropore channels, blocking the micropore channels and leading to a decrease of the micropore volume.

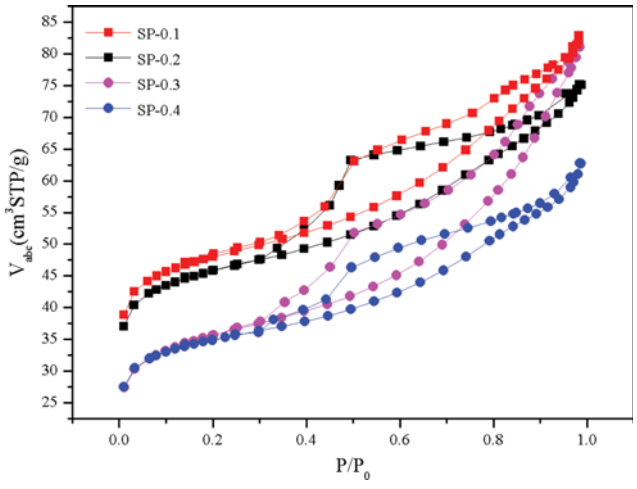

Fig. 4. N_2 adsorption-desorption isotherms of SAPO-11 samples.

The N_2 adsorption-desorption isotherms of as-synthesized samples are shown in Fig. 4. The typical N_2 adsorption-desorption isotherms of as-synthesized are of the type IV isotherm according to the IUPAC classification. High adsorption of N_2 occurred in the low relative pressure range and obvious hystereses are detected, suggesting the existence of micropores and the secondary mesopores in samples with the different Si content. A hysteresis between adsorption and desorption branches can be observed at medium relative pressure (0.3-1.0) for all the samples, which demonstrates the presence of a large number of secondary mesopores. Fig. 5 shows the micropores and secondary mesopores size distributions of the SAPO-11 samples. Generally speaking, the secondary mesopores probably result from SAPO-11 microcrystalline piled up in the synthesis process. Although Fig. 5(b) shows that pore volume at 50 nm for SP-0.3 is the highest, Fig. 4 shows that the secondary mesopores of SP-0.2 are still the largest. So the secondary mesopores size distribution decreases in the order of SP-0.2>SP-0.3>SP-0.1>SP-0.4 (see Fig. 4 and Fig. 5).

1-6. NH_3-TPD and ^{29}Si MAS NMR

NH_3-TPD is frequently used to determine the number and strength of the acid sites in catalysts. The NH_3-TPD results of as-synthesized samples are presented in Fig. 6. There are two distinct regions at 160-180 °C and 270 °C for all the as-synthesized samples, which indicates that weak and medium acid sites are dominant on SP-0.1, SP-0.2, SP-0.3 and SP-0.4. Fig. 6 shows that the acid strength of as-synthesized samples is qualitatively similar. The total acid number and the medium strength acid number of the samples decrease in the order of SP-0.3>SP-0.2>SP-0.4>SP-0.1, which implies that the Si content in the framework makes a considerable contribution to the acidity of SAPO-11.

^{29}Si MAS NMR spectra are used to investigate the local environments of the Si atoms incorporated into the framework. The ^{29}Si MAS NMR spectra (Fig. 7) show different peaks due to the different Si content of the samples. SP-0.1 shows an intensive peak at −90 ppm assigned to Si(4Al) environments and a weak peak −109

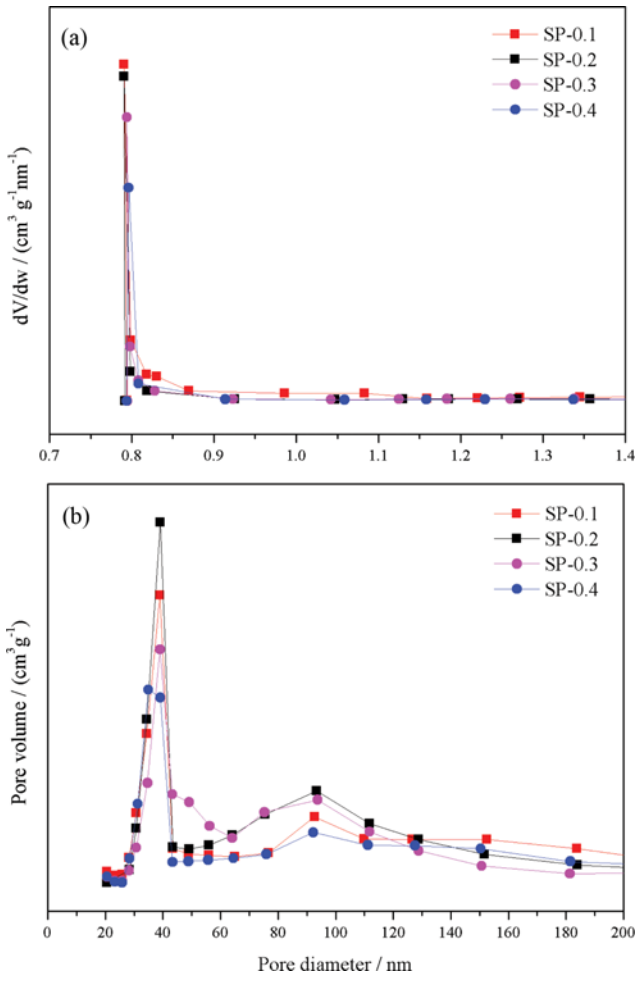

Fig. 5. Pore size distributions of SAPO-11 samples.
(a) Micropores size distributions of SAPO-11 samples; (b) Mesopores size distributions of SAPO-11 samples

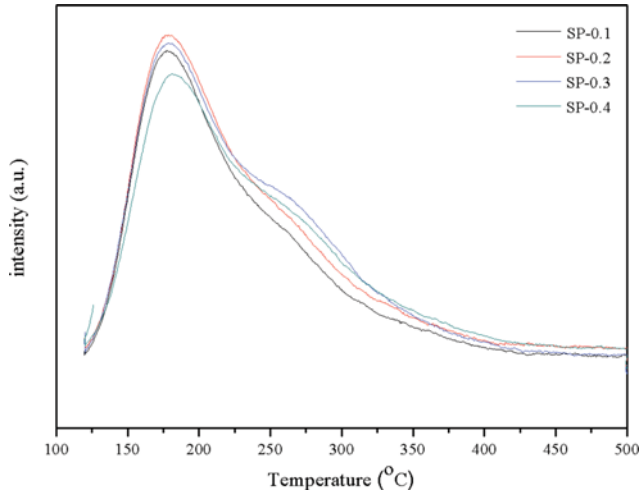

Fig. 6. NH_3-TPD results of SAPO-11 samples.

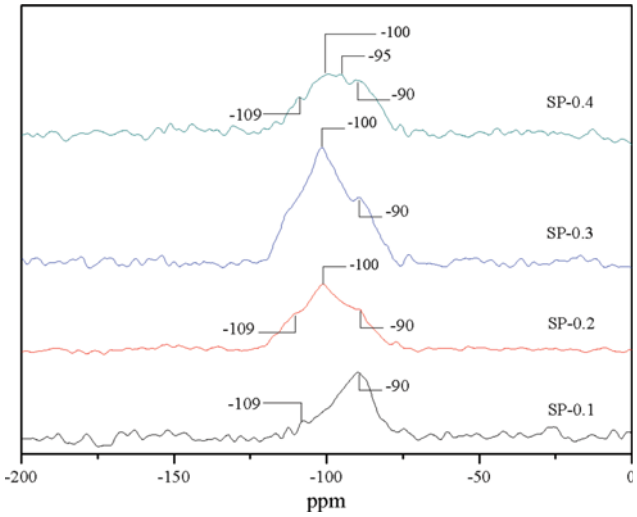

Fig. 7. ^{29}Si MAS NMR spectra of SAPO-11 samples.

Table 3. Gaussian simulation results for the ^{29}Si NMR MAS spectra of SAPO-11 samples

Samples	Selectivity of various environmental Si (%)			
	Si(4Si) −109 ppm	Si(2Al, 2Si) −100 ppm	Si(3Al, 1Si) −95 ppm	Si(4Al) −90 ppm
SP-0.1	39.3	0	0	60.7
SP-0.2	9.6	65.3	0	25.1
SP-0.3	0	51.8	0	48.2
SP-0.4	27.1	22.8	19.7	30.4

ppm assigned to Si(4Si) environments. This also confirms that the Si directly participating in the crystallization or the SM2 substitution mechanism is predominantly for forming Si(4Al) structure by Si-O-Al linkage. There are three peaks at −90, −100 and −109 ppm over SP-0.2, which is induced by the Si(4Al), Si(2Al, 2Si) and Si(4Si) environments, respectively. The ^{29}Si MAS NMR spectrum of SP-0.3 shows the peaks at −90 ppm and −100 ppm, ascribed to the Si(4Al) and Si(2Al, 2Si) environments, respectively. With the SiO_2/Al_2O_3 molar ratio of 0.40, the ^{29}Si MAS NMR spectrum of SP-0.4 shows more resonance peaks at −90, −95, −100 and −109 ppm, which are attributed to Si(4Al), Si(3Al, 1Si), Si(2Al, 2Si) and Si(4Si) environments, respectively. And the ratios of the various types of Si are listed in Table 3.

It is recognized that the Si environments have a significant effect on the acidity of SAPO molecular sieve, which is enhanced in the order of Si(4Si)<Si(4Al)<Si(3Al, 1Si)<Si(2Al, 2Si) [17]. SP-0.1 only has the environments of Si(4Al) and Si(4Si), so the amount of adsorbed NH_3 decreases significantly compared to other samples. Fig. 6 and Table 3 show that SP-0.3 has the most abundant acid sites despite its Si content is not the highest, which is because of its intensive Si(2Al, 2Si) environments. But SP-0.4 has fewer acid sites than SP-0.2 and SP-0.3, which may be because it has lower Si (n Al, 4-n Si, 0<n<4) environments than SP-0.2 and SP-0.3.

1-7. Si Incorporation Mechanism

The XRD (Fig. 1) and SEM (Fig. 2) results show that the crystallinity of SAPO-11 samples is the highest when the SiO_2/Al_2O_3 molar ratio is 0.20 and then the crystallinity of samples reduces with the increase of Si content.

As shown in Fig. 7 (^{29}Si MAS NMR), it is mainly Si(4Al) environments in SP-0.1 that participated in the construction of SAPO-11. With the continuous increase of Si content, the peak at −90 ppm (Si(4Al)) becomes weaker and the others peaks become stronger. These results suggest that Si atoms mainly incorporate into the $AlPO_4$-11 structure by SM2 mechanism in combination with the XRD and SEM results when the Si content is low. Then Si atoms are mainly produced into the $AlPO_4$-11 structure by SM3 mechanism with the increase of Si content. However, when Si content is higher than what the $AlPO_4$-11 structure could accommodate (the SiO_2/Al_2O_3 molar ratio is 0.3 and 0.4), excess Si atoms will be expelled from the framework, and the Si-rich morphous phase will occur in the products, which leads to low crystallinity of SP-0.3 and SP-0.4.

2. Catalytic Performances of the Methylation of Naphthalene

The catalytic conversion and stability of the investigated zeolites are compared in Fig. 8. As shown in Fig. 8, the conversion of naphthalene for SP-0.1 is 70.5% and 22.1% at the reaction time of 1 h and 6 h, respectively. The naphthalene conversion of SP-0.2 is 78.8% at the reaction time of 1 h but only decreases to 46.7% at the reaction time of 6 h. SP-0.3 presents the highest conversion of naphthalene (81.9%) at the reaction time of 1 h and the conversion of naphthalene is 25.5% at the reaction time of 6 h. The conversion of naphthalene for SP-0.4 is 73.4% at the reaction time of 1 h and 13.5% at the reaction time of 6 h. The initial activity of SP-0.3 is higher than the other samples because it has more active centers than others owing to its strong acidity. However, the conversion of naphthalene does not decrease quickly, although its strong acidity could accelerate the coke formation. On the contrary, SP-0.2 exhibits initially lower naphthalene conversion and its stability is the highest among all the zeolites although its acidity is not the weakest. These indicate that there is no a coincidence between the naphthalene conversion and the acidity of samples. Table 2 shows that there is little difference of the surface area among the four SAPO-11 samples. As seen in Fig. 4 and Fig. 5, the secondary meso-

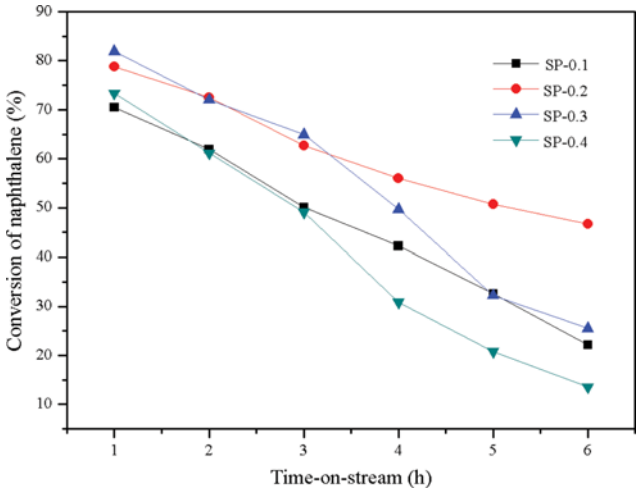

Fig. 8. The conversion of naphthalene over SAPO-11 samples.

Table 4. Comparison of catalytic performance of different SAPO-11 samples in the methylation of naphthalene

Sample	Reaction time	Naphthalene conv./%	Product distribution			Selectivity of 2,6-DMN	2,6-/2,7-DMN	2,6-DMN yield/%
			MN	DMN	TMN			
SP-0.1	1 h	70.5	41.7	39.6	19.7	20.1	0.91	4.91
	6 h	22.1	50.7	28.1	21.2	33.2	1.52	2.10
SP-0.2	1 h	78.8	38.6	49.2	12.2	29.1	1.10	6.30
	6 h	46.7	48.9	37.6	13.5	48.2	1.72	3.80
SP-0.3	1 h	81.9	38.7	43.6	17.7	22.7	0.98	5.20
	6 h	25.5	47.3	32.6	20.1	34.0	1.61	2.23
SP-0.4	1 h	73.4	42.6	32.8	24.6	19.4	0.90	4.35
	6 h	13.5	53.6	20.1	26.3	31.6	1.21	0.86

Reaction conditions: Temperature=400 °C, pressure=0.1 MPa, WHSV (based on naphthalene)=0.19 h^{-1}, n (naphthalene) : n (methanol) : n (mesitylene)=1 : 5 : 3.5 (molar ratio), time-on-stream=1 h, 6 h

pore size distributions decrease as SP-0.2>SP-0.3>SP-0.1>SP-0.4. Thus, the increased second mesoporosity can introduce more reactants into the major channels or can facilitate the products desorbing out of the major channels, thus resulting in the enhancement of the conversion of naphthalene of SP-0.2. Therefore, the conversion of naphthalene is probably related to the differences in the pore structure of SAPO-11 samples, especially relating to the amount of secondary mesopores in the SAPO-11 zeolite. The more amount of secondary mesoporses in the SAPO-11 zeolite, the higher conversion of naphthalene over SAPO-11 sample is obtained. Meanwhile, from Fig. 8, the naphthalene conversion over all the samples decreases with the prolonging of reaction time. It is possibly because some of the reactant molecules or the intermediates form in the pore channels during the synthesis process, which block the pores channels of SAPO-11 samples and prevent the further diffusion of the reactant and the product molecules [18], thus leading to the low naphthalene conversion at longer reaction time. Based on the above reason, the authors think that the naphthalene conversion increases with increasing time because the pore size of SAPO-11 zeolites can be enlarged, through changing synthetic method or modifying the SAPO-11 zeolites [19-21].

The catalytic performance of the investigated zeolites with 1 h and 6 h time on stream (TOS) is listed in Table 4. Table 4 shows that the main products are methylnaphthalene (MN), dimethylnaphthalene (DMN) and trimethylnaphthalene (TMN). The 2,6-DMN yield over the investigated zeolites decreases in the order of SP-0.2>SP-0.3>SP-0.1>SP-0.4. The selectivity of 2,6-DMN and 2,6-/2,7-DMN ratio decreases in the order of SP-0.2>SP-0.3>SP-0.1>SP-0.4 in the reaction time, which is not associated with the acidity of the samples. Fang et al. [22] have calculated that 2,6-DMN is somewhat larger than 2,7-DMN in molecular dimension, with their molecular dimensions in length, thickness and cylindrical diameter being 10.06 Å, 2.76 Å, 6.44 Å for 2,6-DMN and 9.73 Å, 2.76 Å, 6.03 Å for 2,7-DMN, respectively. Therefore, 2,6-DMN suffers more diffusion resistance than 2,7-DMN diffusing out from the pore channel of SAPO-11. SP-0.2 exhibits broader pore size distributions than the other SAPO-11 samples (see Fig. 4 and Fig. 5). The broad pore size distributions are helpful for the diffusion of 2,6-DMN, particularly the generation of the secondary mesopores over SP-0.2, which makes it more favorable to the diffusion of 2,6-DMN, thus finally leading to higher selectivity of 2,6-DMN and 2,6-/2,7-DMN ratio. So SAPO-11 zeolite with more amount of secondary mesoporses presents higher selectivity of 2,6-DMN and 2,6-/2,7-DMN ratio than other SAPO-11 samples.

CONCLUSIONS

Different SAPO-11 samples were synthesized using different Si content under hydrothermal conditions. It was found that Si content in the starting gel had crucial effect on the physicochemistry properties of SAPO-11 samples, and then influenced their catalytic performances in the methylation of naphthalene. The experimental results proved that SAPO-11 synthesized with SiO_2/Al_2O_3 ratio of 0.2 showed the highest crystallinity, the broadest pore size distributions and the highest catalytic performances among all the SAPO-11 samples synthesized in this study.

ACKNOWLEDGEMENTS

This work was supported by the National High-tech R&D Program of China (863 Program) (2012AA051002).

REFERENCES

1. C. S. Song and H. H. Schobert, *Fuel. Process. Technol.*, **34**, 157 (1993).
2. T. Tsutsui, K. Ijichi, T. Inomata, Setiadi, T. Kojima and K. Sato, *Chem. Eng. Sci.*, **59**, 3993 (2004).
3. D. Fraenkel, M. Cherniavsky, B. Ittah and M. Levy, *J. Catal.*, **101**, 273 (1986).
4. J. N. Park, J. Wang, C. W. Lee and S. E. Park, *Bull. Korean Chem. Soc.*, **23**, 1011 (2002).
5. G. Pazzuconi, G. Terzoni, C. Perego and G. Bellussi, *Stud. Surf. Sci. Catal.*, **135**, 4071 (2001).
6. X. F. Bai, K. Y. Sun, W. Wu, P. F. Yan and J. Yan, *Appl. Catal. A.*, **375**, 279 (2010).
7. J. Wen, G. Y. Wang, Y. Zhang, Z. G. Qiu and L. F. Zhao, *Petrochemical. Technology*, **39**(5), 487 (2010).
8. X. X. Wang, J. Wen, W. Zhang, L. F. Zhao and W. Wei, *Petrochemical. Technology*, **41**(11), 1284 (2012).
9. B. M. Lok, C. A. Messina, R. L. Patton, R. T. Gajek, T. R. Cannon

and E. M. Flanigen, *Crystalline silicoaluminophosphates*, US. 4440871 (1984).
10. C. M. Song, Y. Fengf and L. L. Ma, *Micropor. Mesopor. Mater.*, **147**, 205 (2012).
11. R. Roldán, M. Sánchez, G. Sankar, F. J. Romero-Salguero and C. Jiménez-Sanchidrián, *Micropor. Mesopor. Mater.*, **99**, 288 (2007).
12. X. T. Ren, N. Liu, J. Q. Cao, Z. Y. Liu and S. Y. Xiang, *Appl. Catal. A.*, **298**, 144 (2006).
13. P. Mériaudeau, V. A. Tuan, V. T. Nghiem, S. Y. Lai, L. N. Hung and C. Naccache, *J. Catal.*, **169**, 55 (1997).
14. C. M. Chen and J. M. Jehng, *Catal. Lett.*, **85**, 73 (2003).
15. T. C. Xiao, L. D. An and H. L. Wang, *J. Mol. Catal.*, **8**, 429 (1994).
16. P. Mériaudeau, V. A. Tan, S. Y. Lai, L. N. Hung and C. Naccache, *J. Catal.*, **169**, 55 (1997).
17. G. Saster, D. W. Lewis, C. Richard and A. Catlow, *J. Phys. Chem. B.*, **101**, 5249 (1997).
18. N. Lucas, A. Bordoloi, A. P. Amurute, P. Kasinathan, A. Vinu, W. Bohringer, J. C. Q. Fletcher and S. B. Halligudi, *Appl. Catal. A.*, 74 (2009).
19. P. Liu, J. Ren and Y. H. Sun, *Chinese J. Catal.*, **29**, 379 (2008).
20. A. K. Sinha, S. Seelan, S. Tsubota and M. Haruta, *Top. Catal.*, **29**, 95 (2004).
21. I. Eswaramoorthi and N. Lingappan, *J. Mol. Catal. A: Chem.*, **218**, 229 (2004).
22. Y. M. Fang and H. Q. Hu, *Catal. Commun.*, **7**, 264 (2006).